

# Magnetothermal and magnetorotational instabilities in hot accretion flows

De-Fu Bu<sup>1\*</sup>, Feng Yuan<sup>1†</sup> and James M. Stone<sup>2</sup>

<sup>1</sup>*Key Laboratory for Research in Galaxies and Cosmology, Shanghai Astronomical Observatory, Chinese Academy of Sciences, 80 Nandan Road, Shanghai 200030, China*

<sup>2</sup>*Department of Astrophysical Sciences, Peyton Hall, Ivy Lane, Princeton, NJ 08544, USA*

17 January 2011

## ABSTRACT

In a hot, dilute, magnetized accretion flow, the electron mean-free path can be much greater than the Larmor radius, thus thermal conduction is anisotropic and along magnetic field lines. In this case, if the temperature decreases outward, the flow may be subject to a buoyancy instability (the magnetothermal instability, or MTI). The MTI amplifies the magnetic field, and aligns field lines with the radial direction. If the accretion flow is differentially rotating, the magnetorotational instability (MRI) may also be present. Using two-dimensional, time-dependent magnetohydrodynamic simulations, we investigate the interaction between these two instabilities. We use global simulations that span over two orders of magnitude in radius, centered on the region around the Bondi radius where the infall time of gas is longer than the growth time of both the MTI and MRI. Significant amplification of the magnetic field is produced by both instabilities, although we find that the MTI primarily amplifies the radial component, and the MRI primarily the toroidal component, of the field, respectively. Most importantly, we find that if the MTI can amplify the magnetic energy by a factor  $F_t$ , and the MRI by a factor  $F_r$ , then when the MTI and MRI are both present, the magnetic energy can be amplified by a factor of  $F_t \cdot F_r$ . We therefore conclude that amplification of the magnetic energy by the MTI and MRI operates independently. We also find that the MTI contributes to the transport of angular momentum, because radial motions induced by the MTI increase the Maxwell (by amplifying the magnetic field) and Reynolds stresses. Finally, we find that thermal conduction decreases the slope of the radial temperature profile. The increased temperature near the Bondi radius decreases the mass accretion rate.

**Key words:** accretion, accretion discs – conduction – magnetohydrodynamics: MHD – ISM: jets and outflow – black hole physics

## 1 INTRODUCTION

Hot, diffuse accretion flows are likely present in low-luminosity active galactic nuclei (AGN) and the quiescent and hard states of black hole X-ray binaries (Narayan 2005; Yuan 2007; Narayan & McClintock 2008). When the mass accretion rate is very low, the electron mean-free path will be very large, so the accreting plasma is nearly collisionless. For example, from *Chandra* observations of the accretion flow at the Galactic Center, Sgr A\*, the electron mean-free path is estimated to be 0.02 – 1.3 times the Bondi radius ( $\sim 10^5 - 10^6$  Schwarzschild radii). In such cases, thermal

conduction can have significant influence on the dynamics (Quataert 2004; Johnson & Quataert 2007), resulting in the transport of thermal energy from the inner (hotter) to the outer (cooler) regions. If the energy flux carried by thermal conduction is substantial, the temperature of the gas in the outer regions can be increased above the virial temperature. Thus, gas in the outer regions is able to escape from the gravitational potential of the central black hole and form outflows, significantly decreasing the mass accretion rate (Tanaka & Menou 2006; Johnson & Quataert 2007).

Time-dependent hydrodynamical simulations of hot accretion flows show that they are convectively unstable, no matter whether the flow is radiatively inefficient (Igumenshchev & Abramowicz 1999; Stone, Pringle & Begelman 1999; Igumenshchev & Abramowicz 2000) or efficient (Yuan

\* E-mail:dfbu@shao.ac.cn

† E-mail:f yuan@shao.ac.cn

& Bu 2010). This is consistent with the prediction of one-dimensional analytical models of advection-dominated accretion flows (ADAFs; Narayan & Yi 1994; 1995). Convective instability occurs because the entropy of the flow increases in the direction of gravity. However, in a magnetized weakly collisional accretion flow, in which the electron mean-free path is much greater than the Larmor radius, thermal conduction is anisotropic and primarily along magnetic field lines. In this case, Balbus (2000; 2001) found that the stability criterion for convection is fundamentally altered: convection occurs when the temperature – not the entropy – increases in the direction of gravity. Convective instabilities in this regime are referred to as the magnetothermal instability (MTI).

In a weakly magnetized, non-rotating atmosphere, local simulations have demonstrated that the MTI can amplify the magnetic field and lead to a substantial convective heat flux (Parrish & Stone 2005; 2007). Sharma, Quataert & Stone (2008; hereafter SQS08) investigated the effects of the MTI on accretion flows in two-dimensions using global simulations in spherical polar coordinates. Their simulations focused on the region around the Bondi radius, where the MTI growth time is shorter than gas infall time. They found the MTI can amplify the magnetic field and align field lines with the direction of the temperature gradient (radially), consistent with the results obtained by previous local simulations. The effects of the MTI on the intracluster medium (ICM) have also been investigated (Parrish, Stone & Lemaster 2008). In that study also, the MTI drives the magnetic field lines to be radial, leading to a conductive flux which is an appreciable fraction of the classical Spitzer value. Such a high rates of thermal conduction make the slope of the temperature profile flatter.

The studies of the MTI described above all focus on a non-rotating accretion flow. It is well-known that in a weakly magnetized, differentially rotating hot accretion flow, the magnetorotational instability (MRI; Balbus & Hawley 1991; 1998) will be present, and MHD turbulence driven by the MRI is thought to be the most promising mechanism of angular momentum transport. In principle the MTI and MRI should coexist in such flows. Therefore, an interesting question for investigation is whether the MTI and MRI interact with one another, i.e., does one instability enhance or suppress the other, or do the two instabilities operate entirely independently. For example, it is of interest to ask whether convective motions driven by the MTI can transport angular momentum, and similarly whether turbulent motions driven by the MRI can transport heat.

Motivated by the question above, we present the results of two-dimensional magnetohydrodynamical (MHD) simulation of hot accretion flows with anisotropic thermal conduction and rotation. We investigate flows which are slowly rotating (not rotationally supported) at the Bondi radius, where the growth time of both the MTI and MRI is shorter than the infall time. This paper is organized as follows: we introduce our numerical methods and initial conditions in Section 2, most of our results are presented in Section 3, while Section 4 is devoted to a summary and discussion.

## 2 NUMERICAL SIMULATION

We adopt two-dimensional, spherical coordinates  $(r, \theta)$  and assume axisymmetry  $\partial/\partial\phi \equiv 0$ . We use the Zeus-2D code (Stone & Norman 1992a, 1992b) to solve the MHD equations with anisotropic thermal conduction:

$$\frac{d\rho}{dt} + \rho \nabla \cdot \mathbf{v} = 0, \quad (1)$$

$$\rho \frac{d\mathbf{v}}{dt} = -\nabla p - \rho \nabla \psi + \frac{1}{4\pi} (\nabla \times \mathbf{B}) \times \mathbf{B}, \quad (2)$$

$$\frac{\partial \mathbf{B}}{\partial t} = \nabla \times (\mathbf{v} \times \mathbf{B}), \quad (3)$$

$$\rho \frac{d(e/\rho)}{dt} = -p \nabla \cdot \mathbf{v} - \nabla \cdot \mathbf{Q}, \quad (4)$$

$$\mathbf{Q} = -\chi \hat{\mathbf{b}} (\hat{\mathbf{b}} \cdot \nabla) T. \quad (5)$$

Here  $\rho$  is the mass density,  $\mathbf{v}$  is the velocity,  $p$  is the pressure,  $\psi = -GM/r$  is the gravitational potential ( $G$  is the gravitational constant and  $M$  is the mass of the central black hole),  $\mathbf{B}$  is the magnetic field,  $e = p/(\gamma - 1)$  is the internal energy ( $\gamma$  is the adiabatic index),  $\mathbf{Q}$  is the heat flux along magnetic field lines,  $\chi$  is the thermal diffusivity,  $\hat{\mathbf{b}}$  is the unit vector along magnetic field and  $T$  is the temperature of the gas.

**For convenience, we adopt  $\chi = \kappa p/T$  and assume that  $\kappa = a_c (GMr)^{1/2}$  which has the dimension of a diffusion coefficient ( $\text{cm}^2 \text{s}^{-1}$ ).** Anisotropic thermal conduction is implemented using the method based on limiters (Sharma & Hammett 2007) to guarantee that heat always flows from hot to cold regions.

We initialize our simulations as follows. The radial velocity, internal energy, and density of the accretion flow are adopted from the hydrodynamic Bondi solution. For the other two components of the velocity ( $v_\theta$  and  $v_\phi$ ), we set  $v_\theta = 0$  and  $v_\phi = l_0/r$  with  $l_0 (= \text{const.})$  (a parameter of our simulations) the specific angular momentum of the accretion flow. The initial magnetic field is uniform and perpendicular to the equatorial plane, (i.e.  $\mathbf{B} = B_z$ , where  $z$  is the vertical cylindrical coordinate). We have run four models. The parameters used in these models are listed in Table 1. In models L1 and L2, we set  $l_0$  to be 0.1 times the Keplerian angular momentum at the inner boundary. Thus, in models L1 and L2, the centrifugal barrier is inside our inner boundary, and rotationally supported region is never formed in these two models. In models H1 and H2, however, we set  $l_0$  to be 10 times the Keplerian angular momentum at the inner boundary. Thus, in models H1 and H2, the centrifugal barrier is outside our inner boundary, so that a rotationally supported disk can form, which is subject to the MRI. We set  $\beta$  (the ratio of gas pressure to magnetic pressure) to be  $\beta = 10^{12}$  at the outer boundary in our initial conditions. We assume that the adiabatic index  $\gamma = 1.5$ . We use the Bondi radius,  $r_B = GM/c_\infty^2$  ( $c_\infty$  is the sound speed at infinity and we set  $c_\infty^2 = 10^{-6} c^2$  where  $c$  is the speed of light) to normalize all of the length scales in our paper. Times reported in this paper are all in the unit of the inverse rotation frequency at the outer radius of the domain,  $\Omega_{out}^{-1} = [r_{out}^3/GM]^{1/2}$ .

All of our calculations span a domain bounded by an inner boundary at  $r_{in} = 0.05r_B$  and an outer boundary at  $20r_B$ . As in SQS08, we adopt a numerical resolution of  $60 \times 44$ . The radial grid is logarithmically spaced. A uniform polar grid extends from  $\theta = 0$  to  $\pi$ . At the poles, we use

**Table 1.** Parameters for all of our models

Models	$l_0^\dagger$	$a_c^\ddagger$	description
L1	$0.1l_{in}$	0	no MTI, no MRI
L2	$0.1l_{in}$	0.2	only MTI
H1	$10l_{in}$	0	only MRI
H2	$10l_{in}$	0.2	with MRI, with MTI

$^\dagger l_0$  is the initial angular momentum of the flow.  $l_{in}$  is the Keplerian angular momentum at the inner boundary.

$^\ddagger \chi = \kappa p/T$  is the thermal diffusivity and  $\kappa = a_c(GMr)^{1/2}$ .

axisymmetric boundary conditions. In the radial direction, we use inflow/outflow boundary conditions at both the inner and outer boundaries. For the temperature at the inner and outer boundaries, we use outflow boundary conditions.

### 3 RESULTS

#### 3.1 Magnetic field amplification

A weakly magnetized, conductive, differentially rotating accretion flow is subject to magnetothermal and magnetorotational instabilities when the condition,

$$-\frac{1}{\rho} \frac{dp}{dr} \frac{d \ln T}{dr} + \frac{d\Omega^2}{d \ln r} < 0, \quad (6)$$

is satisfied, where  $\Omega$  is the angular velocity of the accretion flow. Provided that the magnetic field is weak, the condition for the existence of MTI alone is

$$-\frac{1}{\rho} \frac{dp}{dr} \frac{d \ln T}{dr} < 0. \quad (7)$$

This condition is always satisfied in the initial conditions of our calculations, thus as long as the MTI growth time is smaller than the gas infall time, the MTI will grow. The condition for the existence of the MRI is

$$\frac{d\Omega^2}{d \ln r} < 0. \quad (8)$$

This condition is again always satisfied in the initial conditions of our calculations. Defining

$$\gamma_{MTI}^2 = \left| -\frac{1}{\rho} \frac{dp}{dr} \frac{d \ln T}{dr} \right|, \quad (9)$$

$$\gamma_{MRI}^2 = \left| \frac{d\Omega^2}{d \ln r} \right|, \quad (10)$$

the MTI and MRI growth timescales are then  $t_{MTI} = \gamma_{MTI}^{-1}$  and  $t_{MRI} = \gamma_{MRI}^{-1}$ , respectively. The wavelength of the maximum growth rate for MTI and MRI are

$$\lambda_{MTI} = 2\pi v_a / \gamma_{MTI} \quad (11)$$

and

$$\lambda_{MRI} = 2\pi v_a / \gamma_{MRI}, \quad (12)$$

respectively. Here  $v_a (\equiv \sqrt{B^2/4\pi\rho})$  is the Alfvén speed.

We investigate the interplay between the MTI and MRI by examining the magnetic field amplification by the two instabilities. Note that in addition to the MTI and MRI, the magnetic field can also be amplified by the geometric convergence of the accretion flow in spherical geometry and flux

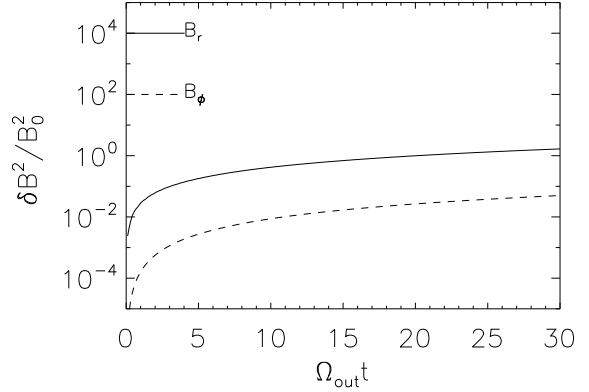


**Figure 1.** Evolution of the volume averaged magnetic energy in both the  $r$  and  $\phi$  components of the magnetic field normalized to the initial magnetic energy in a shell from  $r_{out}/40$  to  $r_{out}$  in model L1. In this model, magnetic field is amplified only by flux freezing. Since  $v_\theta \sim 0$ , there is almost no amplification of the  $\theta$  component of the field, so it is not shown. The growth of each component is defined as  $\delta B_{r,\theta,\phi}^2 = (\langle B_{r,\theta,\phi}^2 \rangle_V - B_{r,\theta,\phi,0}^2)$ , where  $\langle \rangle_V$  denotes volume average and  $B_0$  is the initial field strength.

freezing. First, we investigate the magnetic field amplification by flux freezing by carrying out model L1. We note that in models L1 and L2, the centrifugal barrier is inside our inner boundary, thus the timescale for the MRI to grow is much longer than the gas infall timescale. Furthermore, in model L1 we set the coefficient of the thermal diffusivity  $a_c = 0$ , i.e., there is no MTI in model L1. Therefore, the magnetic field amplification in model L1 can only be due to flux freezing. The results below show that the effect of flux freezing on magnetic field amplification is very small, allowing us to ignore this effect in the analysis of models L2, H1 and H2.

In model L2, we set the coefficient of the thermal diffusivity  $a_c = 0.2$  so that it is unstable to the MTI. In this model, the magnetic field is amplified only by the MTI. In models H1 and H2, the centrifugal barrier is outside our inner boundary. The timescale for the growth of the MRI is much shorter than the gas infall time, so that the MRI will affect the flow in both of these two models. In model H1, we set the coefficient of the thermal diffusivity  $a_c = 0$ , so that the MTI is suppressed and the magnetic field is amplified only by the MRI. In model H2, we set the coefficient of the thermal diffusivity  $a_c = 0.2$ , so that both the MTI and MRI coexist, and the magnetic field is amplified by the nonlinear evolution of both. The properties of the four models are summarized in Table 1. The models demonstrate the interplay between the MTI and MRI. We have also tried various other values of  $a_c$ , and find that changing  $a_c$  by a factor of a few does not affect our results, consistent with the conclusion in SQS08.

Figures 1-4 show the change of magnetic energy as a function of time in these four models. The energy is averaged from  $r = r_{out}/40$  to  $r_{out}$ . The solid, dotted, and dashed lines correspond to the energy in the  $r$ ,  $\theta$ , and  $\phi$  components of the magnetic field, respectively.

Figure 1 shows the magnetic energy evolution in model L1. The field is smoothly amplified by flux freezing. At the end of the simulation, the field is only amplified by a factor of 2. Because  $v_\theta \sim 0$ , there is almost no amplification of the  $\theta$  component of the field. From this model, we can see that the effect of flux freezing on magnetic field amplification is very small.

We now investigate the magnetic field amplification by the MTI (model L2). The only difference between models L1 and L2 is that in the latter we include thermal conduction so that the MTI is present. Fig. 2 shows the evolution of the magnetic energy in model L2, it shows significantly more amplification of the magnetic field in comparison to model L1. This amplification is mainly due to motions driven by the MTI. Initially, the field is rapidly amplified by the MTI. After time  $t = 6$ , the magnetic field ceases to grow exponentially, and the growth rate becomes small, for the following reason. The growth rate of the fastest growing mode of the MTI is given by  $\gamma \simeq [1/\rho][dp/dr][d\ln T/dr]^{1/2}b_\theta$  where  $b_\theta = B_\theta/B$ . The growth rate decreases with time because of the decrease of  $b_\theta$  with time. In this model, we use parameters  $F_{r,t}$ ,  $F_{\theta,t}$  and  $F_{\phi,t}$  to represent the amplification factor of the  $r$ ,  $\theta$  and  $\phi$  components of the magnetic field, respectively. We find

$$F_{r,t} = B_{r,f}^2/B_0^2 \sim 100, \quad (13)$$

$$F_{\theta,t} = B_{\theta,f}^2/B_0^2 \sim 10, \quad (14)$$

$$F_{\phi,t} = B_{\phi,f}^2/B_0^2 \sim 100, \quad (15)$$

where  $B_{r,f}$ ,  $B_{\theta,f}$  and  $B_{\phi,f}$  correspond to the  $r$ ,  $\theta$  and  $\phi$  components of the magnetic field at the end of the simulation, respectively. The radial component of the magnetic field is amplified by the MTI significantly. The MTI saturates by aligning field lines with the temperature gradient (radial direction), which is consistent with the results of previous work (Parrish & Stone 2005; 2007; SQS08). SQS08 found that the magnetic field amplification by MTI is quasi-linear. If the magnetic field is weak initially, MTI can amplify the field by a factor of  $\sim 10 - 30$ , independent of the initial field strength. Our calculation confirms their result.

We investigate field amplification by the MRI in model H1. In this model, we turn off thermal conduction so the MTI does not exist, and the magnetic field amplification must be due to motions driven by the MRI. Figure 3 shows the time evolution of the magnetic energy. Initially ( $t < 16.5$ ), the field is very weak, and at our resolution the fastest growing mode of the MRI is not resolved, so that field amplification occurs primarily by flux freezing. The initial ( $t < 1$ ) rapid amplification of the azimuthal component of the magnetic field is due to shear. At  $t = 16.5$ , the magnetic field strength is amplified by flux freezing to a high enough value that the MRI is resolved, and the field undergoes substantial and rapid amplification by the MRI. To illustrate this point, we define a parameter  $Re = \lambda_{MRI}/\Delta x$ , where  $\Delta x$  is the grid size, which measure how well the MRI is resolved on our numerical grid. Figure 5 shows contours of  $Re$  at  $t = 16.5$ . From this figure, it is clear that unstable wavelengths of the MRI are well resolved at that time. The MRI amplifies the field rapidly, and shortly after  $t = 16.5$  the MRI saturates and the field begins to grow algebraically. Saturation of the MRI can be understood as follows. The condition for MRI to operate is  $k^2 v_a^2 + d\Omega^2/d\ln r < 0$ . After

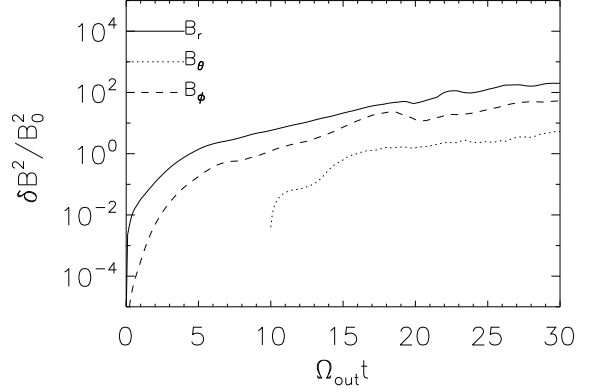


**Figure 2.** Change of volume averaged magnetic energy in the  $r$ ,  $\theta$  and  $\phi$  components of the magnetic field normalized to the initial magnetic energy in a shell from  $r_{\text{out}}/40$  to  $r_{\text{out}}$  as a function of time in model L2. In this model, the magnetic field is amplified by the MTI. The growth of each component of the magnetic field is defined as  $\delta B_{r,\theta,\phi}^2 = (\langle B_{r,\theta,\phi}^2 \rangle_V - B_{r,\theta,\phi,0}^2)$ , where  $\langle \rangle_V$  denotes volume average and  $B_0$  is the initial field strength.

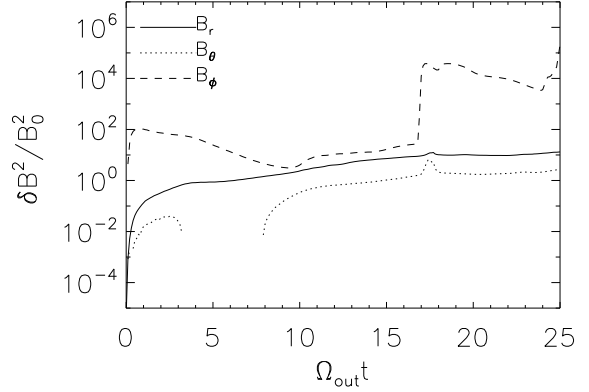


**Figure 3.** Change of volume averaged magnetic energy in the  $r$ ,  $\theta$  and  $\phi$  components of the magnetic field normalized to the initial magnetic energy in a shell from  $r_{\text{out}}/40$  to  $r_{\text{out}}$  as a function of time in Model H1. In this model, magnetic field is amplified by the MRI. The growth of each component of the magnetic field is defined as  $\delta B_{r,\theta,\phi}^2 = (\langle B_{r,\theta,\phi}^2 \rangle_V - B_{r,\theta,\phi,0}^2)$ , where  $\langle \rangle_V$  denotes volume average and  $B_0$  is the initial field strength.

$t = 18$ , we find  $k^2 v_a^2 + d\Omega^2/d\ln r \sim 0$  in the region where the MRI growth wave length can be resolved, so the growth rate of MRI decreases significantly. Using parameters  $F_{r,r}$ ,  $F_{\theta,r}$ , and  $F_{\phi,r}$  to represent the magnetic field amplification factor of the  $r$ ,  $\theta$  and  $\phi$  components of the magnetic field, respectively, we find

$$F_{r,r} = B_{r,f}^2/B_0^2 \sim 10, \quad (16)$$

$$F_{\theta,r} = B_{\theta,f}^2/B_0^2 \sim 10, \quad (17)$$

$$F_{\phi,r} = B_{\phi,f}^2/B_0^2 \sim 10^4, \quad (18)$$



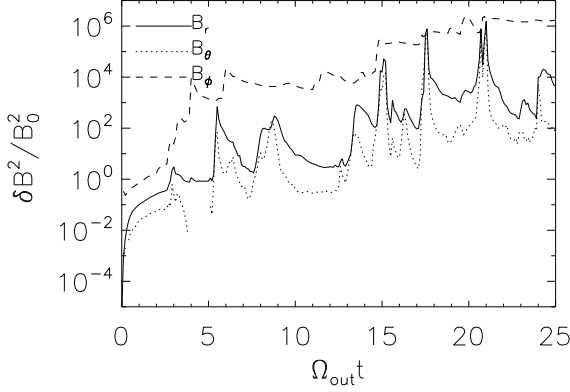


**Figure 4.** Change of volume averaged magnetic energy in the  $r$ ,  $\theta$  and  $\phi$  components of the magnetic field normalized to the initial magnetic energy in a shell from  $r_{\text{out}}/40$  to  $r_{\text{out}}$  as a function of time in Model H2. In this model, magnetic field is amplified by both the MTI and MRI. The growth of each component of the magnetic field is defined as  $\delta B_{r,\theta,\phi}^2 = (\langle B_{r,\theta,\phi}^2 \rangle_V - B_{r,\theta,\phi,0}^2)$ , where  $\langle \rangle_V$  denotes volume average and  $B_0$  is the initial field strength.

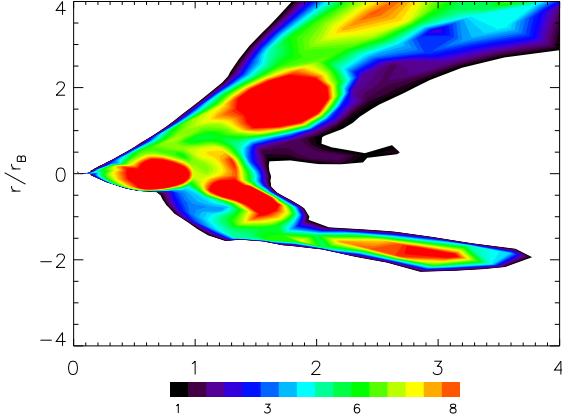


**Figure 5.** Contour of  $Re = \lambda_{\text{MRI}}/\Delta x$  at time  $t = 16.5$ , where  $\Delta x$  is the grid size. It is clear that the wavelength of the fastest growing mode of the MRI is well resolved at time  $t = 16.5$ .

where  $B_{r,f}$ ,  $B_{\theta,f}$  and  $B_{\phi,f}$  correspond to the  $r$ ,  $\theta$  and  $\phi$  components of the magnetic field at the end of the simulation, respectively. The toroidal component is most significantly amplified as expected.

In model H2, we turn on thermal conduction so both the MTI and MRI coexist. Figure 4 shows the time evolution of the magnetic energy. Initially ( $t < 3$ ), there is only the MTI. This is because initially the field is too weak for unstable wavelengths of the MRI to be resolved. At  $t = 3$  the magnetic field has been amplified by the MTI enough that unstable modes of the MRI are resolved, and the MRI begins to drive motions. After  $t = 3$ , the field begins to be amplified exponentially by both the MTI and MRI, until at  $t \sim 20$  both instabilities saturate and the growth of the field

becomes algebraic. Using parameters  $F_r$ ,  $F_\theta$  and  $F_\phi$  to represent the amplification factor of the  $r$ ,  $\theta$  and  $\phi$  components of the magnetic energy, respectively, we find

$$F_r = B_{r,f}^2/B_0^2 \sim 10^3, \quad (19)$$

$$F_\theta = B_{\theta,f}^2/B_0^2 \sim 100, \quad (20)$$

$$F_\phi = B_{\phi,f}^2/B_0^2 \sim 10^6, \quad (21)$$

where  $B_{r,f}$ ,  $B_{\theta,f}$  and  $B_{\phi,f}$  correspond to the  $r$ ,  $\theta$  and  $\phi$  components of the magnetic field at the end of the simulation, respectively.

Comparing models L2, H1 and H2, we find,

$$F_r \sim F_{r,t} \cdot F_{r,r}, \quad (22)$$

$$F_\theta \sim F_{\theta,t} \cdot F_{\theta,r}, \quad (23)$$

$$F_\phi \sim F_{\phi,t} \cdot F_{\phi,r}. \quad (24)$$

Let us first consider the amplification of the radial component of the magnetic field. If the MTI alone amplifies the radial component of the magnetic energy by a factor of  $F_{r,t}$  (model L2), and the MRI alone by a factor of  $F_{r,r}$  (model H1), then when the MTI and MRI coexist the radial component of the magnetic field can be amplified by a factor of  $F_{r,t} \cdot F_{r,r}$  (model H2). The amplification factors for the other two components of the magnetic energy behave similarly. We therefore conclude that in the nonlinear regime the MTI and MRI amplify the field independently, most likely because the MTI is buoyancy instability driven by radial gradients in the temperature, while the MRI is a dynamical instability driven by the radial gradient of the orbital frequency. Provided that the magnetic field is weak and the plasma is dilute, thermal conduction from hotter to cooler regions will make the plasma buoyantly unstable, regardless of whether the flow also contains turbulent eddies driven by the MRI. On the other hand, provided that the magnetic field is weak and differential rotation exists, the MRI can operate regardless of the presence of convective eddies driven by the MTI.

### 3.2 The role of MTI in angular momentum transfer

The MRI is now believed to be the most promising mechanism of angular momentum transport in fully ionized accretion flows. It is interesting to investigate whether the MTI can contribute to angular momentum transfer in hot, diffuse accretion flows.

We first compare the angular momentum profiles in models L1 and L2 at the end of both calculations. The flow in model L1 is laminar, while there is (only) MTI in model L2. Angular momentum profiles at the end of the simulations are shown in Figure 6. It is clear that the angular momentum distribution of model L1 is almost the same as the initial distribution. This is because the flow in model L1 is laminar, and the magnetic field is very weak: therefore both the Reynolds and magnetic stresses are very small and there is almost no angular momentum transfer. It is also clear that in model L2, angular momentum is transferred from the inner to the outer regions. In order to investigate the mechanism for the angular momentum transport in this case, we plot the Maxwell and Reynolds stresses in Figure 7.

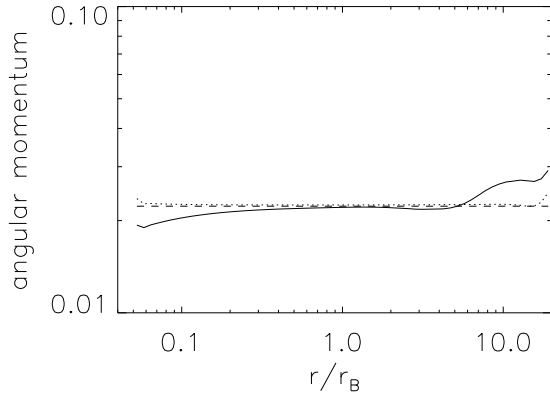


**Figure 6.** Radial profiles of specific angular momentum for models L1 (dotted line) and L2 (solid line). The dashed line shows the initial angular momentum distribution.

The dotted and solid lines correspond to the Maxwell stress ( $-B_r B_\phi / 4\pi$ ) in models L1 and L2, respectively. Because of magnetic field amplification by the MTI, the Maxwell stress in model L2 is much larger than that in model L1. The triangles and squares denote the Reynolds stress in models L1 and L2 respectively. Due to the presence of motions driven by the MTI in model L2, the Reynolds stress is three orders of magnitude higher than in model L1. Because the magnetic field is still very weak in model L2, the Maxwell stress is much smaller than the Reynolds stress. We conclude the angular momentum transport in model L2 is dominated by the Reynolds stress. We note that although the MTI induced Reynolds stress does transfer angular momentum, the effect is quite low, so that there is only a small change of the angular momentum profile compared to the initial conditions.

Next we compare the angular momentum distribution in models H1 and H2 at late times in Figure 8. Both profiles are quite similar. Recall that both models are unstable to the MRI, while only H2 is unstable to the MTI. The similarity in the angular momentum profiles indicates that the role of the MTI in angular momentum transport is less important compared to the MRI.

### 3.3 Effects of MTI on the structure of the accretion flow

Figure 9 shows the time-averaged density (upper-left panel), temperature (upper-right) and mass accretion rate (lower panel) for models H1 and H2. In the upper panels, the solid and dashed lines correspond to models H1 and H2, respectively. In the lower panel, the solid, dotted and dashed lines correspond to the net accretion rate, inflow rate and outflow rate, respectively. The black and red lines correspond to models H1 and H2, respectively. As shown in the upper-right panel, the radial profile of temperature in model H2 (with MTI) is flatter than that in model H1. This is likely because thermal conduction transports energy from the inner to the outer regions of the flow. From the lower panel, we can see that the inflow rate decreases due to the effects of thermal conduction. This is consistent with Johnson &

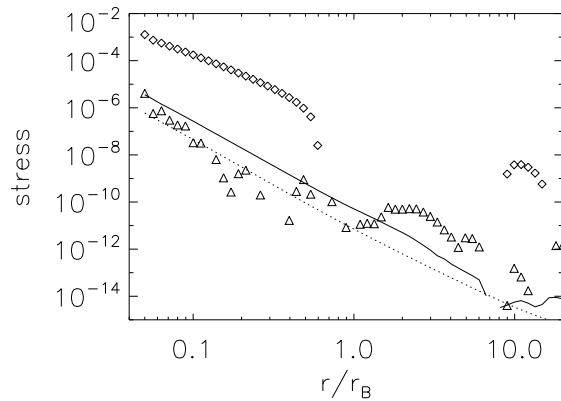


**Figure 7.** Radial profiles of stress. The dotted and solid lines correspond to the Maxwell stress in models L1 and L2, respectively. The triangle and square are Reynolds stress in models L1 and L2, respectively.

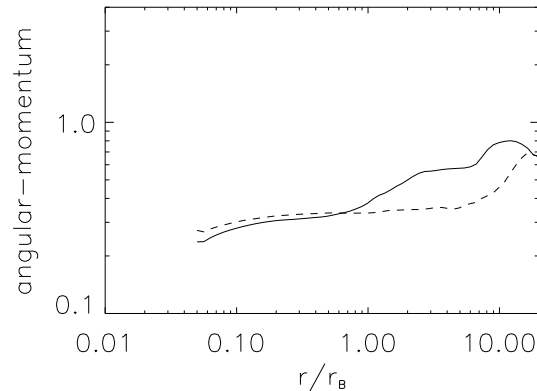


**Figure 8.** Radial profiles of specific angular momentum for models H1 (solid line) and H2 (dashed line).

Quataert (2007). The decrease is caused by the increased heating of the outer regions by thermal conduction.

## 4 SUMMARY AND DISCUSSION

In extremely low accretion rate systems, the plasma is very dilute, the collisional mean-free path of electrons is much greater than their Larmor radius; thus thermal conduction is anisotropic and along magnetic field lines. Anisotropic thermal conduction can fundamentally alter the Schwarzschild convective instability criterion. Convection sets in when temperature (as opposed to entropy) increases in the direction of gravity. Convective instability in this regime is referred to as the magnetothermal instability (MTI). The MTI can amplify the magnetic field and align field lines with the temperature gradient (i.e., the radial direction). If the flow has angular momentum, the MRI may also exist. We have investigated the possible interaction between the MTI and

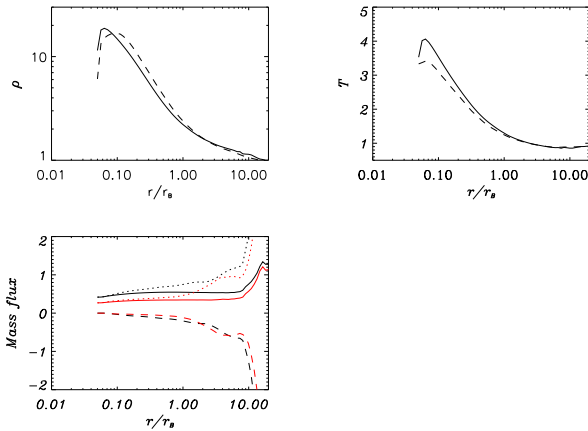


**Figure 9.** Radial profiles of time-averaged variables in models H1 and H2. Upper-left and upper-right panels correspond to the radial profiles of density and temperature, respectively. In the upper panels, solid and dashed lines correspond to models H1 and H2, respectively. In the lower panel, the solid, dotted and dashed lines correspond to the net accretion rate, inflow rate and outflow rate, respectively. The black and red lines correspond to models H1 and H2, respectively.

MRI by performing two-dimensional magnetohydrodynamical (MHD) simulations of nonradiative rotating accretion flows with anisotropic thermal conduction.

We have presented the results from four models, with focus on the amplification of magnetic energy by the combination of MTI and MRI. As a control case, we computed a model (L1) in which neither the MTI nor the MRI was present, so that the magnetic field is amplified only by flux freezing and geometrical compression in the flow. We find that field amplification via flux freezing in this case is very small. Next, we investigated the effects of the MTI on magnetic field amplification in model L2. We find that the MTI can amplify magnetic field significantly, which is consistent with the result obtained in previous work. Finally we considered the evolution of rotating flows that are unstable to the MRI. In model H1 (no thermal conduction), only the MRI is present. In model H2, both the MTI and MRI coexist. By comparing the structure and evolution of these different models, we find that if the MTI alone can amplify the magnetic energy by a factor of  $F_t$ , and the MRI alone by a factor of  $F_r$ , then when the MTI and MRI are both present, the magnetic energy can be amplified by a factor of  $F_t \cdot F_r$ . Thus, we conclude that the MTI and MRI operate independently, and that there is little feedback on the amplification factor in the nonlinear regime. Because the MTI and MRI are driven by different properties of the flow (temperature gradient in the case of the former, and angular velocity gradient in the case of the latter), the presence of one may not strongly affect the presence of the others. Thus, anisotropic thermal conduction can make the plasma buoyantly unstable, regardless of whether or not turbulent eddies driven by the MRI are present. Similarly, an unstable rotation profile can result in the MRI, regardless of whether or not there are convective eddies induced by the MTI.

In addition to the interplay between the MTI and MRI, we have also investigated the effects of MTI on angular mo-

mentum transport. We find that the MTI enhances angular momentum transport simply because it can amplify magnetic field (thus enhancing the Maxwell stress) and induce radial motions (thus enhancing the Reynolds stress). But we note that the effects of the MTI on angular momentum transfer are small. Finally, we find that thermal conduction does make the slope of the temperature smaller due to the outward transport of energy, and the increase of the temperature in the outer regions decreases the mass accretion rate.

Lastly, we would like to mention that in a weakly collisional accretion flow, the ion mean-free path can be much greater than its Larmor radius; thus the pressure tensor is anisotropic. In this case, the growth rate of the MRI can increase dramatically at small wavenumbers compared to the MRI in ideal MHD (Quataert, Dorland & Hammett 2002; Sharma, Hammett & Quataert 2003). In this regime, the viscous stress tensor is anisotropic, and Balbus (2004; see also Islam & Balbus 2005) has shown that when anisotropic viscosity is included, the flow is subject to the magnetoviscous instability (MVI). The MVI may also amplify magnetic field significantly. An interesting project for the future is to investigate the effects of the MVI on hot accretion flows.

## 5 ACKNOWLEDGMENTS

We thank P. Sharma for sending us his code. This work was supported in part by the Natural Science Foundation of China (grants 10773024, 10833002, 10821302, and 10825314), the National Basic Research Program of China (973 Program 2009CB824800), and the CAS/SAFEA International Partnership Program for Creative Research Teams.

## REFERENCES

- Balbus S. A., 2000, *ApJ*, 534, 420
- Balbus S. A., 2001, *ApJ*, 562, 909
- Balbus S. A., 2004, *ApJ*, 616, 857
- Balbus S. A., Hawley J. F., 1991, *ApJ*, 376, 214
- Balbus S. A., Hawley J. F., 1998, *Rev. Mod. Phys.*, 70, 1
- Igumenshchev I. V., Abramowicz M. A., 1999, *MNRAS*, 303, 309
- Igumenshchev I. V., Abramowicz M. A., 2000, *ApJS*, 130, 463
- Islam T., Balbus S., 2005, *ApJ*, 633, 328
- Johnson B. M., Quataert E., 2007, *ApJ*, 660, 1273
- Narayan R., 2005, *Ap&SS*, 300, 177
- Narayan R., McClintock J.E., 2008, *New Astron. Rev.*, 51, 733
- Narayan R., Yi I., 1994, *ApJ*, 428, L13
- Narayan R., Yi I., 1995, *ApJ*, 452, 710
- Parrish I. J., Stone J. M., 2005, *ApJ*, 633, 334
- Parrish I. J., Stone J. M., 2007, *ApJ*, 664, 135
- Parrish I. J., Stone J. M., Lemaster N., 2008, *ApJ*, 688, 905
- Quataert E., 2004, *ApJ*, 613, 322
- Quataert E., Dorland W., Hammett G. W., 2002, *ApJ*, 577, 524
- Sharma P., Hammett G. W., 2007, *J. Comp. Phys.*, 227, 123
- Sharma P., Hammett G. W., Quataert E., 2003, *ApJ*, 596, 1121
- Sharma P., Quataert E., Stone J. M., 2008, *MNRAS*, 389, 1815
- Stone J.M., Norman M. L., 1992a, *ApJS*, 80, 753
- Stone J.M., Norman M. L., 1992b, *ApJS*, 80, 791
- Stone J.M., Pringle J. E., Begelman M. C., 1999, *MNRAS*, 310, 1002
- Tanaka T., Menou K., 2006, *ApJ*, 649, 345
- Yuan F., 2007, in Luis C. Ho., Jian-Min Wang, eds, *ASP conf.*

Ser., Vol.373, The Central Engine of Active Galactic Nuclei.

Astron. Soc. Pac., San Francisco, p.95

Yuan F., Bu D. F., 2010, MNRAS, 408, 1051